RSC Advances

ROYAL SOCIETY OF CHEMISTRY

www.rsc.org/advances

Journal Name

RSCPublishing

ARTICLE

Electrodeposition and Characterization of Ni-SiC Composite Coatings from Deep Eutectic Solvent

Cite this: DOI: 10.1039/x0xx00000x

Ruiqian Li,[ab] Qingwei Chu[ab] and Jun Liang*[a]

Received ooth January 2012,
Accepted ooth January 2012

DOI: 10.1039/x0xx00000x

www.rsc.org/

In this paper, a choline chloride (ChCl)/ethylene glycol (EG) based deep eutectic solvent (DES) without any stabilizing additives was used as electrolyte to electrodeposit Ni matrix composite coatings containing either micro or nano-sized SiC particles. The electrochemical behaviour of Ni in the presence of micro or nano-sized SiC particles was investigated. The effects of particle concentration, current density and stirring rate on the content of micro or nano-sized SiC particles incorporated into the Ni matrix were investigated. The microstructure, microhardness and tribological property of pure Ni and Ni matrix composite coatings containing micro or nano-sized SiC particles were compared. Results showed that the addition of micro or nano-sized SiC particles have significant effects on the nucleation mechanism of Ni in ChCl/EG DES. Micro and nano-sized SiC particles uniformly incorporated into the composite coatings, the content of SiC particles embedded in Ni coatings depends on the deposition parameters and particle size, and the maximum content of SiC in composite coatings can achieve 12.80 wt.% and 5.37 wt.%, respectively. Compared with the pure Ni coating, the microhardness and wear resistance of Ni-SiC composite coatings are significantly improved and the Ni matrix composite coatings containing nano-sized SiC particles exhibited better tribological property than that containing the micro-sized SiC particles.

1 Introduction

Metal matrix composite coatings (MMCs) generally exhibited wide engineering applications owing to their excellent properties, such as wear resistance, self-lubrication, corrosion resistance and oxidation resistance.[1-5] Electrodeposition is a simple and effective method to fabricate MMCs. Up to now, the electrodeposition of MMCs containing different second-phase particles, such as hard oxides (Al_2O_3,[2,6] CeO_2,[7,8] TiO_2[9,10]), carbides (SiC,[11,12] WC[13,14]), solid lubricates (MoS_2,[15,16] graphite,[4] PTFE[17]), diamond[18] and carbon nanotube,[19,20] have been widely studied. However, the poor dispersion stability of the particles in plating bath and the low content of the particles in matrix metals are two key issues for the electrodeposition of MMCs from aqueous solutions, so uniform and massive deposition of the second-phase particles in the MMCs is a difficult task without the addition of surfactants or dispersants. The homogeneous dispersion of the second-phase particles in an electrolyte is a key factor to obtained composite coatings with excellent properties. Therefore, it is consistently interesting to find a compatible solvent which could stably disperse the second-phase particles.

Recent decades, ionic liquids (ILs) have been used as alternative solvents for electrodepositing metals and composites due to their excellent properties, including wide potential windows, high solubility of metal salts, high ionic conductivity, good thermal stability and negligible vapor pressure.[21] In particular, the ILs generally own higher viscosity and ionic strength than the aqueous solution, which is beneficial to the codeposition process of metal matrix composites.[21] The high viscosity of ILs could effectively decrease the setting velocity of solid particles and improve the stability of particles in the plating bath. The high ionic strength of ILs can also weaken the interaction of solid particles and prevent the agglomeration of particles in electrolyte. To date, however, ILs are still difficult to achieve large-scale application, mainly due to its high moisture susceptibility, high cost, complex preparation and purification process. Moreover, some ILs are toxic and environment-unfriendly. Deep eutectic solvents (DESs) are a

[a] State Key Laboratory of Solid Lubrication, Lanzhou Institute of Chemical Physics, Chinese Academy of Sciences, Lanzhou 730000, People's Republic of China. E-mail: jliang@licp.cas.cn.
[b] Graduate University of Chinese Academy of Sciences, Beijing 100049, People's Republic of China.

new type of IL, which was firstly found by Abbott and co-workers.[22] DESs not only have the advantages of ILs, but also are moisture and air stable, cheap, green and easy to synthesis. Therefore, DESs are considered to be promising solvents for electrodepositing metal coatings.

Abbott et al.[23] firstly studied the possibility of electrodeposition of composite coatings in two kinds of DESs (ChCl:2EG and ChCl:2Urea) in 2007. In their work, the deposition behavior of copper-matrix[24] and silver-matrix[25] composite coatings in the DESs with micro and nano-sized particles (Al_2O_3 and SiC) was studied. The results showed that the Al_2O_3 and SiC particles with different sizes can be stably dispersed in the DESs without any additives and stirring. The maximum content of particles incorporated in composite coating can achieve 27.3 wt.%. Martis et al.[26] reported that multiwalled carbon nanotubes (MWCNTs) could be well dispersed in ChCl:2Urea DES more than 30 days and homogenously co-deposited with nickel matrix. You et al.[17] found that the PTFE particles, which were very difficult to disperse in aqueous solution, could be stably dispersed in the ChCl:2EG DES without additives. The obtained Ni-PTFE composite coatings showed much higher wear resistance than pure Ni coating. All these aforementioned works made clear that the DESs can be used as a suitable solvent for codeposition process and have shown a promising application in electrodepositing high quality MMCs.

Although many metal matrix composites coating have been deposited from different ILs, remarkably little is known about the basic science, such as the double layer structure, mechanisms of particles stability and metals nucleation/growth, in contrast to the corresponding aqueous systems. The majority of investigations on codeposition process in aqueous solutions have suggested that three global factors, namely (1) the applied current density, (2) the particle type and concentration and (3) bath agitation or electrode movement, can be identified as influencing the composite coating characteristics.[27] To our best knowledge, however, rarely attention has been paid to the effects of these experimental parameters in DESs on the codeposition process and coating properties. Most notably, the size of the second-phase particles is one of the important influencing factors for the process of electrodeposition and properties of metal composite coatings. In addition, as one of the most commonly used MMCs, the Ni matrix composite coatings deposited from DESs was rarely reported.

In this work, ChCl:2EG DES was used as the solvent to electrodeposit Ni matrix composite coatings containing either micro or nano-sized SiC particles by pulse current. The electrochemical behaviour and nucleation/growth mechanism of Ni codeposition process with different sizes of SiC particles were discussed. The influence of particle concentration, current density and stirring rate on the content of SiC particles with different sizes in composite coating was investigated. In particular, the effect of micro or nano-sized SiC particles on the texture, morphology and tribological performance of Ni matrix composite coatings was explored in detail.

2 Experimental Sections

2.1 Preparation of Deep Eutectic solvent

Choline Chloride [$HOC_2H_4N(CH_3)_3Cl$] (ChCl, Aldrich 99%), Ethylene Glycol [$C2H_6O_2$] (EG, Aldrich 99%) were used as received. The eutectic mixture was prepared by mixing ChCl and EG with a molar ratio of 1:2 at 70 ℃ until a homogeneous, colourless liquid formed. Then 0.2 M $NiCl_2 \cdot 6H_2O$ was added into the DES and stirred until a transparent green liquid was obtained. SiC particles with different sizes (0.3 μm and 40 nm) were used without any pre-treatment. In order to keep the particles well dispersed in the electrolyte, the bath was stirred by a magnetic stirrer for 24 h. The suspension was subsequently dispersed by ultrasonic agitation for 1 h before all experiments.

2.2 Electrochemical tests

Cyclic voltammetric (CV) and chronoamperometric (CA) tests were carried out using an Autolab PGSTAT302N potentiostat/galvanostat. A three-electrode system, with a platinum microelectrode (2 mm×0.1 mm) as the working electrode, a platinum disc electrode (1 mm diameter) as the counter electrode and an Ag wire as the reference electrode, was used to perform the electrochemical tests. The working electrode and counter electrode were polished with 0.3 μm alumina paste, cleaned with acetone and deionized water by an ultrasonic cleaner before each experiment. Cyclic voltammograms were carried out at scan rates between 10 and 50 mV/s. All electrochemical tests were performed at 70 ℃.

2.3 Electrodeposition process

The electrodeposition of Ni-SiC composite coatings was carried out in ChCl:2EG DES by pulse current. The compositions of the Ni-SiC plating bath and deposition conditions are shown in Table 1. A piece of pure Ni plate was used as the anode and a copper plate (30 mm×7 mm) was used as the cathode. The distance between the anode and cathode was 50 mm. The copper plate was polished with 800#, 1200# and 1500# sandpaper, cleaned in acetone and deionized water for 10 min, activated in 5 wt.% HCl for 30 s before the electrodeposition process. The plating bath was agitated during electrodeposition process with a magnetic stirrer.

2.4 Coating characterization

The morphology and elemental composition of the Ni and Ni-SiC composite coatings were observed using scanning electron microscopy (SEM, JEOL, JSM-5600LV) with energy dispersive spectroscopy (EDS, Kevex). The SiC content values are quoted in weight percent and represent the average of five measurements. The cross-sectional morphologies were determined by optical microscope (ZEISS, Axio). X-ray diffraction analyses were carried out by a D/MAX-2400 (Rigaku, Japan) with a Cu-Kα target (λ=0.15406 nm) at a scan rate of 5 °/min. The target voltage and the tube current were 40 KV and 150 mA, respectively. The Vickers hardness of pure Ni and Ni-SiC composite coatings were measured by a microhardness tester (HXD-1000B) at a load of 25 g and

indentation time of 5 s. The wear tests were carried out under dry sliding conditions in ambient air by a ball-on-plate type CSM tribometer. An AS14 steel ball (d=6 mm) was used as the counter body with a load of 2 N. The slide distance was 5 mm, the slide time was 10 min and the number of cycles was 1200. The wear morphology and wear loss of the coatings were measured by SEM and 3D Profiler (NonoMap 500LS, AEP Technology).

3 Results and discussion

3.1 Effect of SiC particles on the electrochemical behavior of Ni(II) in ChCl:2EG DES

Fig. 1 shows the cyclic voltammetric curves of Ni(II) in the ChCl:2EG DES without and with micro or nano-sized SiC particles. The effects of different sized SiC particles on the cyclic voltammograms are shown in Fig. 1a. The reduction potential of Ni(II) shifted towards negative direction and its peak current decreased when the micro or nano-sized SiC particles are added into the DES. The decrease of peak current was mainly attributed to the decrease of the Ni(II) concentration on the electrode surface[25] or the electrode surface area due to physical blocking by the insulating SiC particles.[24] It can also be found that the cyclic voltammetric curves of Ni(II) in the DES with addition of micro or nano-sized SiC particles have classical nucleation loops, which were often found in the metal deposition process on a heterogeneous substrates. In this case, the deposition process needs higher overpotential to initiate metal nucleation.[28] There are two anodic peaks in all three voltammograms, which can be attributed to two different stripping processes corresponded to the morphology of metals being deposited from bulk electrolytic deposition at more positive potential and under potential deposition at less positive potential.[24] It should be noted that the anodic response of Ni(II) in the ChCl:2EG DES with nano-sized SiC particles (annotated as "*n*SiC") is quite similar to that in the ChCl:2EG DES without SiC particles, which includes a marked peak at more positive potential and a small shoulder at less positive potential. For the Ni(II) in the ChCl:2EG DES with micro-sized SiC particles (annotated as "*m*SiC"), however, there are two distinct peaks in the anodic branch and the current of the less positive peak is higher than that of the more positive peak, indicating that the addition of micro-sized SiC particles is advantageous to underpotential deposition (UPD) of Ni.

Fig. 1b and 1c shows the CVs for the reduction of Ni(II) in ChCl:2EG DES with *m*SiC and *n*SiC particles on a Pt electrode as a function of scan rate. Along with increasing scan rate, the reduction peak potentials negatively shifted and the peak currents increased. The cathodic peak currents (i_{pc}) were plotted against the square root of potential scan rate ($\nu^{1/2}$) and good linear relationships were obtained (presented as inserts in Fig. 1b and 1c, respectively). In addition, the straight line does not pass through the origin. These results indicated that the deposition process is controlled by diffusion and kinetic limitations.[29] It should also be noted that there is only one Ni stripping peak in the CV curve at lower scan rates for Ni(II) in ChCl:2EG DES with *m*SiC particles as shown in Fig. 1b. At higher scan rates, however, UPD peaks appeared, suggesting that the higher scan rate is conducive to under potential deposition of Ni in the ChCl:2EG DES with *m*SiC particles.

To study the nucleation/growth mechanism of electrodeposited Ni in ChCl:2EG DES without and with micro or nano-sized SiC particles, chronoamperometric (CA) tests were performed under a series of step potentials. The current-time transients are illustrated in Fig. 2. It can be seen that the tendencies of all the current-time transient curves are similar irrespective of the presence of the SiC particles. The abrupt drop of current is caused by the double layer charging and the following increase of current is attributed to the formation and growth of Ni nuclei. And then the current decreases regularly after reaching a maximum current (i_m) at a time (t_m). The shape of current-time curves indicates a typical diffusion-limited nucleation process with three-dimensional growth of nuclei.[30,31] From the Fig. 2, it is clearly seen that the i_m increases and the t_m shortens with the potential turns negative, which indicated that the increase of overpotential can promote the nucleation process.[32] When comparing the i_m and the t_m under the same potential in Fig. 2a-c, it can be seen that the presence of SiC particles in ChCl:2EG DES resulted in the decrease of i_m and the increase of t_m. This further illustrated that the effective nucleation area of electrode surface decreased when the non-conductive SiC particles adsorbed on the electrode surface.[24] It is generally known that the micro-particles are more easily absorbed on the electrode than the nano-particles. So the *m*SiC particles have a greater influence on the nucleation/growth process than the *n*SiC particles.

Many theoretical models of the electrocrystallization process have been proposed[30] and one of the most famous models was put forward by Scharifker and Hills.[33] The model has two limiting types: three-dimensional instantaneous nucleation and three-dimensional progressive nucleation. The expressions of instantaneous (Eq. (1)) and progressive (Eq. (2)) nucleation are represented, respectively, by

$$\left(i/i_m\right)^2 = 1.9542(t/t_m)^{-1}\left\{1-\exp\left[-1.2564(t/t_m)\right]\right\}^2 \quad (1)$$

$$\left(i/i_m\right)^2 = 1.2254(t/t_m)^{-1}\left\{1-\exp\left[-2.3367(t/t_m)\right]\right\}^2 \quad (2)$$

The experimental transients were normalized to $(i/i_m)^2$ and (t/t_m), compared the non-dimensional plots with theoretical models.

Fig. 3a shows the nucleation/growth process of Ni in ChCl:2EG DES. The results indicate the nucleation fits most closely to a three-dimensional (3D) progressive mechanism when the applied potential is relatively positive (-0.64V). The nucleation mode gradually inclines to a 3D instantaneous mechanism with negative shift of potential. These results agree well with Gómez's report.[34] When the *m*SiC particles were added into the ChCl:2EG DES, the nucleation mechanism of Ni

initially conforms to the 3D instantaneous nucleation, then deviates from the theoretical model. Similar result was obtained for the electrodeposition behaviour of Zn in ChCl:2EG DES.[35] The nucleation of the Ni in ChCl:2EG DES with *n*SiC particles, however, most closely fits the 3D instantaneous nucleation. Therefore, the *m*SiC and *n*SiC particles showed different effects on Ni nucleation/growth mechanism, which is mainly attributed to the size of the particles affects the thickness of electrical double layer and the surface charge of particles.[35]

3.2 Effect of electrodeposition parameters on the SiC content in the composite coatings

The effects of the particle concentration, current density and stirring rate on the micro or nano-sized SiC content in composite coatings were investigated and the results are shown in Fig. 4. It can be seen that the *m*SiC and *n*SiC contents incorporated into Ni matrix with the particle concentration, current density and stirring rate exhibit the same change trends, i.e., the SiC contents in the composite coatings increase to maximum and then decrease. Fig. 4a shows that the SiC contents increase with the increase of particles concentration when the concentration of SiC particles in the solution is lower than a certain threshold value. But once the particle concentration in the solution exceeded the certain threshold value, the content of SiC incorporated into coatings decreases. According to Guglielmi's two-step adsorption model,[36,37] the adsorption rate of SiC particles significantly increased with the particle concentration in aqueous solution, resulting in the particle content in the composite coatings correspondingly increased. When the SiC concentration exceeded the threshold value, however, the agglomeration of the SiC particles takes place more easily due to the poor wettability and high surface free energy and the amount of SiC particles embedded in the Ni matrix decreased. It was believed that the SiC particles in the DES had similar behaviour to that in aqueous solution. Nano-particles are more inclined to agglomerate because of its higher surface energy, so the concentration threshold value of *n*SiC particles (20 g/L) is less than *m*SiC particles (25 g/L). The maximum content of *m*SiC and *n*SiC particles in composite coatings is 12.80 wt.% and 5.37 wt.%, respectively, which means that the large size particles are more easily to incorporate into the Ni matrix.

The relationship between current density and micro or nano-sized SiC contents in the coatings is shown in Fig. 4b. At lower current density, the reduction rate of Ni(II) is relatively slow, making the inert particles have plenty of time to adsorb on electrode surface and were incorporated into the Ni matrix.[5] However, the SiC content in coatings decreases with the further increase of the current density because the reduction rate of Ni(II) is far beyond the adsorption of inert particles, resulting in fewer particles are incorporated into the Ni matrix.[38] The threshold value of current density to obtain maximum content of particles in the composite coating from ChCl:2EG DES with *m*SiC particles is the same as that from the DES with *n*SiC particles.

For the effect of the stirring rate (Fig. 4c), the dispersibility of SiC particles in the electrolyte is enhanced with the increasing of stirring rate, which is beneficial to the increase of the SiC content in the coating. While the particles adsorbed on the electrode surface could be easily removed by the strong turbulent flow at higher stirring rate, resulting in the SiC content in the coatings decrease.[38] It should also be noted that the threshold value of stirring rate to obtain highest SiC content from the ChCl:2EG DES with *n*SiC particles is larger than that from the solution with *m*SiC particles because the surface energy and the number density of nano-sized particles is higher than micro-sized particles under the same concentration. In the composite electrodeposition, the effects of stirring rate on the particles content incorporated into matrix were rarely investigated in DESs. These results clearly showed that the stirring rate has great influence on particles content incorporated into metal matrix in DESs, similar to that in aqueous solution.

3.3 Composition and microstructure of Ni-SiC composite coatings

According to the results in Section 3.2, the electrodeposition parameters with particle concentration of 25 g/L, current density of 5 mA/cm^2 and stirring rate of 1000 rpm were the optimum conditions to obtain a Ni composite coating with higher content of SiC particles. The following context focuses on the characterization of the coatings obtained from these parameters. Fig. 5 shows the XRD patterns of the pure Ni coating, Ni-*m*SiC and Ni-*n*SiC composite coatings. The diffraction peaks at 44.6°, 52.2°, 76.8°and 93.3° are respectively attributed to (111), (200), (220) and (311) crystalline planes of Ni. The diffraction peak of SiC phase can be identified at 2θ angle of 35.4° from Fig. 5b and c, which means that the SiC particles were successfully incorporated into the Ni matrix.

The grain size of pure Ni and Ni-SiC composite coatings were calculated by Debye-Scherrer Equation (reference to (111) and (200) reflection). The results show that the grain size of pure Ni coating is about 25.1nm. However, the grain size of Ni-*m*SiC and Ni-*n*SiC composite coatings decreased to 16.8nm and 13.2nm respectively. The grain size generally depends on the nucleation rates and growth rates, the high nucleation rates and small growth rates are in favoured of refining matrix crystals. In our experiments, the grain refinement of Ni matrix can be ascribed to the decrease of growth rates owing to the embedment of SiC particles in the Ni crystals that seriously hindered crystal boundary migration[39].

Fig. 6 displays the surface morphologies of pure Ni coating and Ni-SiC composite coatings. It can be clearly seen that the Ni-*m*SiC and Ni-*n*SiC composite coatings had quite different microstructure from the pure Ni coating. Fig. (6a and a') shows that the pure Ni coating exhibits nodular particles with the sizes range from 10 μm to 15 μm, and some cracks can be seen on the coating surface. The Ni-*m*SiC composite coating is characterized by a flower-like morphology as presented in Figure 6 (b and b'). The Ni-*n*SiC composite coating is

composed of granular-like structure with a size about 1 μm (Fig. 6 c and c'). Compared with pure Ni coating, the composite coatings are homogeneous and compact in microstructure and the particle size evidently decreased. These results indicated that the incorporation of SiC particles into the Ni matrix exerted strong influence on its microstructure. Similar conclusions were also obtained in the other studies of metal matrix composite coatings,[40-42] but the origin of the influence of particle size on the microstructure is not yet understood. The different deposition behaviour of Ni (corresponding to the different oxide peaks of CV curves presented in section 3.1) may be one of the reasons.

The optical cross-sectional images of pure Ni coating, Ni-*m*SiC and Ni-*n*SiC composite coatings are shown in Fig. 7. All the coatings are compact, uniform and crack-free. The thickness decreases with the order of pure Ni coating, Ni-*n*SiC coating and Ni-*m*SiC coating, which means that the presence of SiC particles in the solution inhibits the growth rate of Ni. It is evident from the Fig.7b and c that micro or nano-sized SiC particles were uniformly incorporated into the Ni coatings. Some larger particles can be observed in the cross-sectional images of composite coatings, suggesting that the SiC particles were agglomerate in the electrodeposition process due to high surface free energy.

3.4 Tribological properties

Fig. 8 shows the friction coefficient of pure Ni coating, Ni-*m*SiC and Ni-*n*SiC composite coatings under dry sliding conditions. The averaged friction coefficient of pure Ni coating is about 0.76. However, the averaged friction coefficients of Ni-*m*SiC and Ni-*n*SiC composite coatings decreased to 0.57 and 0.42, respectively. The decrease of friction coefficient can be attributed to the hard SiC particles in composite coatings reducing the direct contact between metal matrix and counterpart steel ball. The occurrence of the rolling friction with the SiC particles removed from the composite coatings is also beneficial to decreasing the friction coefficient.[43]

The microhardness of pure Ni coating, Ni-*m*SiC and Ni-*n*SiC composite coatings were measured and the results are shown in Fig. 9. It can be seen that the microhardness of Ni-*m*SiC and Ni-*n*SiC composite coatings (716 HV and 895 HV, respectively) are much higher than that of the pure Ni coating (about 289 HV). The increase of the microhardness is clearly related to the hardening effects (particles strengthening, dispersal strengthening and grain refining) of SiC particles in the coating,[44] the nano-sized SiC particles exhibits more evident hardening effect than the micro-sized particles. In addition, it should be noted that the measured microhardness of Ni-SiC composite coatings is higher than that of aqueous solution,[45,46] suggesting that the electrodeposit in DES benefits to obtain the composite coatings with high tribological performance.

The morphology of the worn surfaces of the pure Ni coating, Ni-*m*SiC and Ni-*n*SiC composite coatings were shown in the Fig. 10. For the pure Ni coating (Fig. 10a and a') the surface is characterized by heavy plastic deformation and deep plough grooves along the sliding direction, indicating that the wear mechanism of the pure Ni coating is mainly adhesive wear. The plastic deformation is caused by smearing of wear debris on the counterpart steel ball. The worn surfaces for both the Ni-*m*SiC and Ni-*n*SiC composite coatings are characterized by plastic deformation and some scratches (Fig. 10b and c) and a mixed mechanism of adhesive-abrasive wear can be identified. The plastic deformation zones are obviously decreased for the Ni-SiC composite coatings, and the smallest plastic deformation zones appeared in the Ni-*n*SiC composite coating. This phenomenon can be attributed to the high hardness of Ni-SiC composite coatings.[46] The scratches were probably caused by the SiC particles removed from the Ni-SiC composite coating owing to abrasive wear, and the Ni-*n*SiC composite coating shows a small number of scratches and quite smooth worn areas, due to its higher microhardness than Ni-*m*SiC composite coating.

Fig. 11 shows the two dimensional curves of wear tracks and the wear loss of pure Ni coating, Ni-*m*SiC and Ni-*n*SiC composite coatings after the sliding tests. It is observed from Fig. 11a that the pure Ni coating showed the widest and deepest wear track. The width and depth of wear track for Ni-SiC composite coatings reduced with decreasing the size of SiC particles. Compared to pure Ni coating, the wear loss of the Ni-*m*SiC and the Ni-*n*SiC composite coating is decreased by 70.5% and 88.4%, respectively (Fig. 11b). It is obvious that the higher microhardness and lower friction coefficient of the Ni-*m*SiC and Ni-*n*SiC composite coatings are the main reasons for the decrease of wear loss.

4. Conclusions

This work shows that Ni matrix composite coatings with uniformly distributed micro or nano-sized SiC particles were successfully fabricated by pulse electroplating from ChCl:2EG DES. The size of the SiC particles had a significantly influence on the nucleation/growth process and microstructure of the coatings. The maximum contents of micro and nano-sized SiC particles incorporated into Ni matrix were up to 12.80 wt.% and 5.37 wt.% respectively. The Ni-SiC composite coatings showed excellent wear resistance due to its lower friction coefficient and higher hardness than that of pure Ni coating. And Ni-*n*SiC composite coatings exhibited higher hardness and better wear resistance than Ni-*m*SiC composite coatings.

Acknowledgements

The financial supports from National Natural Science Foundation of China (Grant No. 51305432) and the "Hundred Talents Program" of Chinese Academy of Sciences (J. Liang) were gratefully acknowledged.

References

1 N. K. Shrestha, M. Masuko and T. Saji, Wear, 2003, **254**, 555-564.
2 N. S. Qu, K. C. Chan and D. Zhu, Scr. Mater., 2004, **50**, 1131-1134.
3 K. C. Chan, G. F. Wang, C. L. Wang and K. F. Zhang, Scr. Mater., 2005, **53**, 1285-1290.
4 H. J. Zhao, L. Liu, W. B. Hu and B. Shen, Mater. Des., 2007, **28**, 1374-1378.
5 D. K. Singh and V. B. Singh, Mater. Sci. Eng., A, 2012, **532**, 493-499.
6 H. Gül, F. Kılıç, S. Aslan, A. Alp and H. Akbulut, Wear, 2009, **267**, 976-990.
7 N. S. Qu, D. Zhu and K. C. Chan, Scr. Mater., 2006, **54**, 1421-1425.
8 H. Hasannejad, T. Shahrabi, M. Jafarian and A. S. Rouhaghdam, J. Alloys Compd., 2011, **509**, 1924-1930.
9 S. Spanou, A. I. Kontos, A. Siokou, A. G. Kontos, N. Vaenas, P. Falaras and E. A. Pavlatou, Electrochim. Acta, 2013, **105**, 324-332.
10 Y. H. Zhang, Y. N. Yang, P. Xiao, X. N. Zhang, L. Lu and L. Li, Mater. Lett., 2009, **63**, 2429-2431.
11 A. K. Pradhan and S. Das, J. Alloys Compd., 2014, **590**, 294-302.
12 V. Zarghami and M. Ghorbani, J. Alloys Compd., 2014, **598**, 236-242.
13 S. Mohajeri, A. Dolati and S. Rezagholibeiki, Mater. Chem. Phys., 2011, **129,** 746-750.
14 M. Surender, B. Basu and R. Balasubramaniam, Tribol. Int., 2004, **37**, 743-749.
15 L. Shi, C. F. Sun and W. M. Liu, Appl. Surf. Sci., 2008, **254**, 6880-6885.
16 S. L. Kuo, J. Chin. Inst. Eng., 2004, **27**, 243-251.
17 Y. H. You, C. D. Gu, X. L. Wang and J. P. Tu, Int. J. Electrochem. Sci., 2012, **7**, 12440-12455.
18 T. Tsubota, S. Tanii, T. Ishida, M. Nagata and Y. Matsumoto, Diamond Relat. Mater., 2005, **14**, 608-612.
19 T. C. Lin and B. R. Huang, Sens. Actuators, B, 2013, **185**, 548-552.
20 A. Sun, J. B. Zheng and Q. L. Sheng, Electrochim. Acta, 2012, **65**, 64-69.
21 A. P. Abbott and K. J. McKenzie, Phys. Chem. Chem. Phys., 2006, **8**, 4265-4279.
22 A. P. Abbott, D. Boothby, G. Capper, D. L. Davies and R. K. Rasheed, J. Am. Chem. Soc., 2004, **126**, 9142-9147.
23 A. P. Abbott, G. Capper, K. J. McKenzie and K.S. Ryder, J. Electroanal. Chem., 2007, **599**, 288-294.
24 A. P. Abbott, K. El. Ttaib, G. Frisch, K. J. McKenzie and K. S. Ryder, Phys. Chem. Chem. Phys., 2009, **11**, 4269-4277.
25 A. P. Abbott, K. El. Ttaib, G. Frisch, K. S. Ryder and D. Weston, Phys. Chem. Chem. Phys., 2012, **14**, 2443-2449.
26 P. Martis, V. S. Dilimon, J. Delhalle and Z. Mekhalif, Electrochim. Acta, 2010, **55**, 5407-5410.
27 C. T. J. Low, R. G. A. Wills and F. C. Walsh, Surf. Coat. Technol., 2006, **201**, 371-383.
28 A. H. Whitehead, M. Pölzler and B. Gollas, J. Electrochem. Soc., 2010, **157**, D328.
29 Y. Zheng, K. Dong, Q. Wang, S. J. Zhang, Q. Q. Zhang and X. M. Lu, Sci. China Chem., 2012, **55**, 1587-1597.
30 H. Y. Yang, X. W. Guo, X. B. Chen, S. H. Wang, G. H. Wu, W. J. Ding and N. Birbilis, Electrochim. Acta, 2012, **63**, 131-138.
31 Y. L. Zhu, Y. Katayama and T. Miura, Electrochim. Acta, 2010, **55**, 9019-9023.
32 C. Y. Tan, C. Hang, H. Wei, L. Yu and Z. Q. Zheng, Rare Met. Mater. Eng., 2010, **39**, 0010-0016.
33 B. Scharifker and G. Hills, Electrochim. Acta, 1983, **28**, 879-889.
34 E. Gomez, C. Muller, W. G. Proud and E. Valls, J. Appl. Electrochem. 1992, **22**, 872-876.
35 A. P. Abbott, J. C. Barron, G. Frisch, S. Gurman, K. S. Ryder and A. F. Silva, Phys. Chem. Chem. Phys., 2011, **13**, 10224-10231.
36 N. Guglielm, J. Electrochem. Soc., 1972, **119**, 1009-1012.
37 P. Baghery, M. Farzam, A. B. Mousavi and M. Hosseini, Surf. Coat. Technol., 2010, **204**, 3804-3810.
38 M. R. Vaezi, S. K. Sadrnezhaad and L. Nikzad, Colloids Surf., A, 2008, **315**, 176-182.
39 X. J. Shi, J. M. Wu and G. P. Ling, J. Mater. Sci. Eng., 2012, **30**, 236-240.
40 E. García-Lecina, I. García-Urrutia, J. A. Díez, J. Morgiel and P. Indyka, Sur. Coat. Technol., 2012, **206**, 2998-3005.
41 J. A. Calderón, J. E. Henao and M. A. Gómez, Electrochim. Acta, 2014, **124**, 190-198.
42 A. Lozano-Morales and E. J. Podlaha, J. Electrochem. Soc., 2004, **151**, C478.
43 K. H. Hou and Y. C. Chen, Appl. Sur. Sci., 2011,**257**, 6340-6346.
44 R. K. Saha and T. I. Khan, Sur. Coat. Technol., 2010, 205, 890-895.
45 H. Gül, F. Kılıç, M. Uysal, S. Aslan, A. Alp and H. Akbulut, Appl. Sur. Sci., 2012, **258**, 4260-4267.
46 F. Kılıç, H. Gül, S. Aslan, A. Alp and H. Akbulut, Colloids Surf., A, 2013, **419**, 53-60.

Figure Captions

Fig. 1 Cyclic voltammograms of Ni(II) in ChCl:2EG containing 0.2 M $NiCl_2 \cdot 6H_2O$ (a) with and without SiC particles (scan rate 50 mV/s), (b) with *m*SiC particles and (c) with *n*SiC particles on Pt electrode as function of sweep rate. Inset: the curve of i_{pc} and $v^{1/2}$.

Fig.2 Current-time transients curves from chronoamperometric experiments that were performed at Pt electrode in ChCl:2EG containing 0.2 M $NiCl_2 \cdot 6H_2O$ (a) without SiC particles, (b) with *m*SiC particles and (c) with *n*SiC particles at 70℃.

Fig. 3 Comparison of the dimensionless experimental current-time transients, derived from the results in Fig. 2: (a) without SiC particles, (b) with *m*SiC particles and (c) with *n*SiC particles.

Fig. 4 The effects of (a) particle concentration, (b) current density and (c) stirring rate on micro or nano-sized SiC content in the composite coatings

Fig. 5 XRD patterns of (a) pure Ni coating, (b) Ni-*m*SiC and (c) Ni-*n*SiC composite coating.

Fig. 6 SEM images of (a, a') pure Ni coating, (b, b') Ni-mSiC composite coating and (c, c') Ni-nSiC composite coating.

Fig. 7 Cross-sectional optical images of (a) pure Ni coating, (b) Ni-*m*SiC and (c) Ni-*n*SiC composite coatings.

Fig. 8 Friction coefficient curves of pure Ni coating, Ni-*m*SiC and Ni-*n*SiC composite coatings.

Fig. 9 The microhardness of (a) pure Ni coating, (b) Ni-*m*SiC and (c) Ni-*n*SiC composite coatings.

Fig. 10 SEM images of the wear tracks of (a) pure Ni coating, (b) Ni-*m*SiC and (c) Ni-*n*SiC composite coatings.

Fig. 11 The two dimentional curves (a) and wear loss (b) of wear track for pure Ni coting, Ni-*m*SiC and Ni-*n*SiC composite coatings.

Graphical Abstract

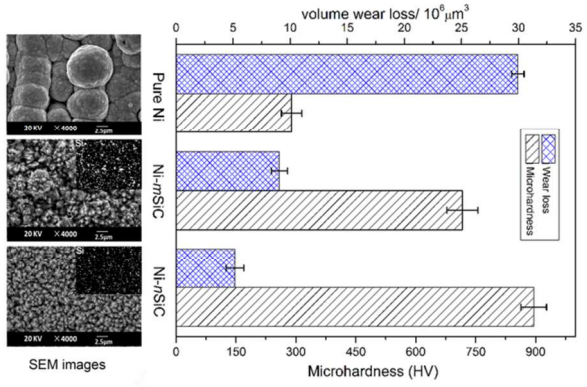

The micro or nano-sized SiC particles have significant effects on nucleation/growth process, morphology, hardness and trilogical performance of Ni coatings.

Fig. 1

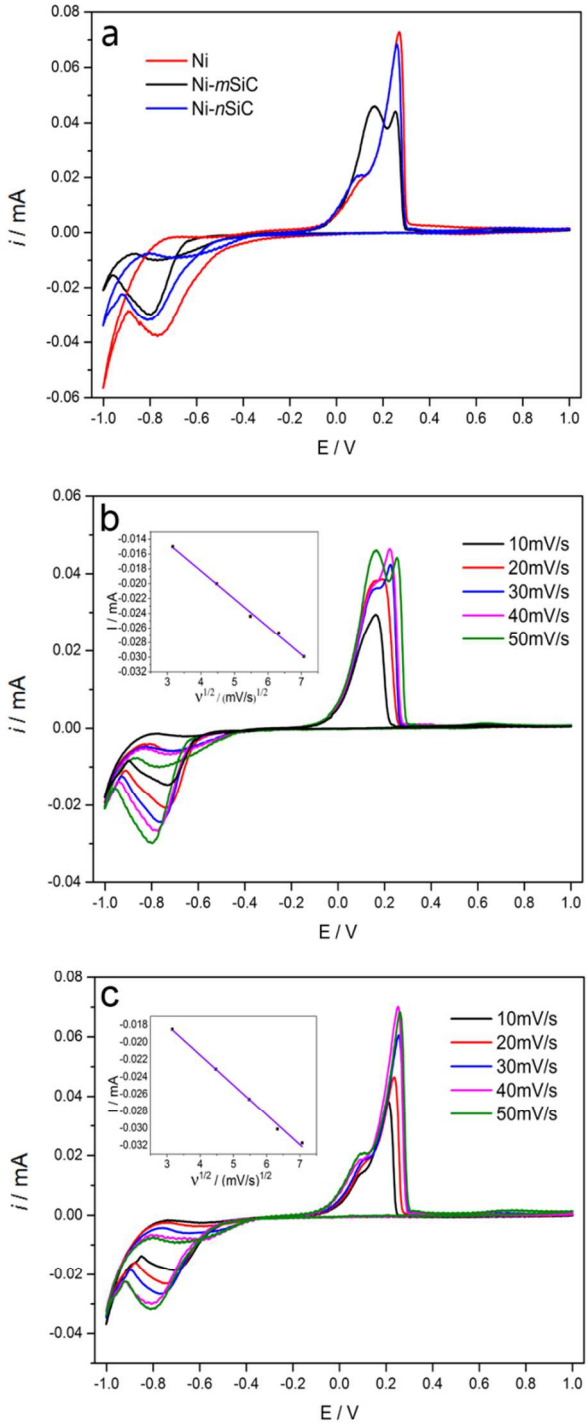

Fig. 2

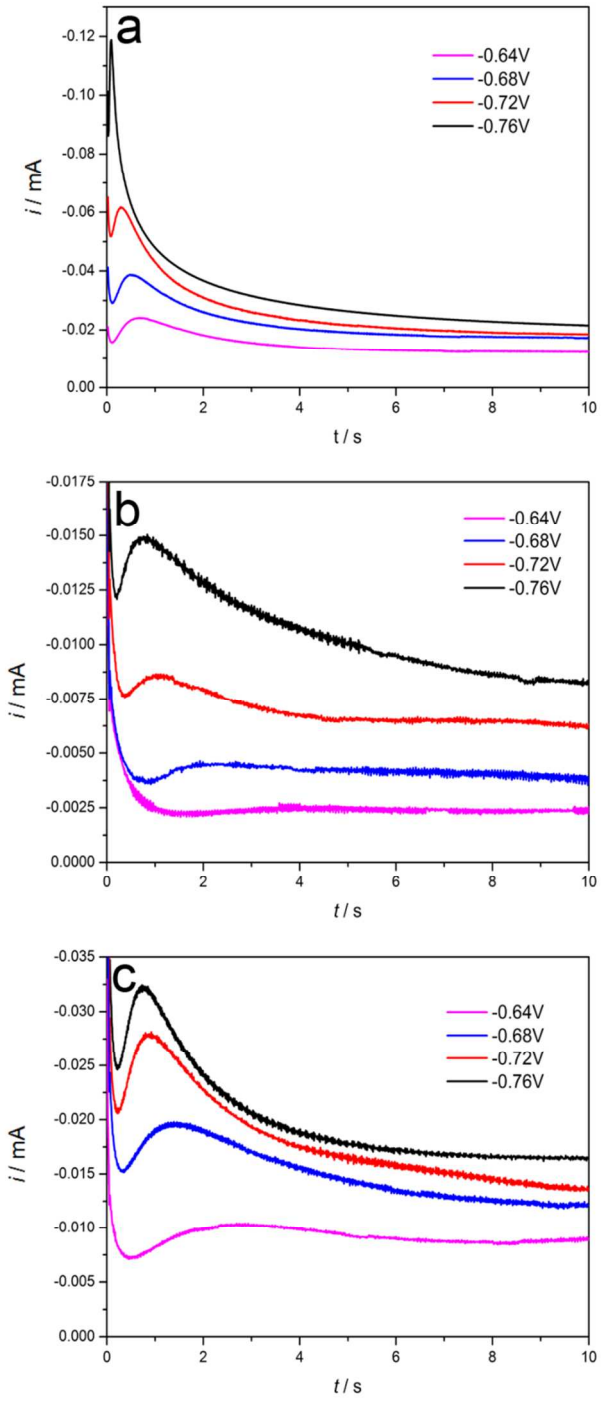

Fig. 3

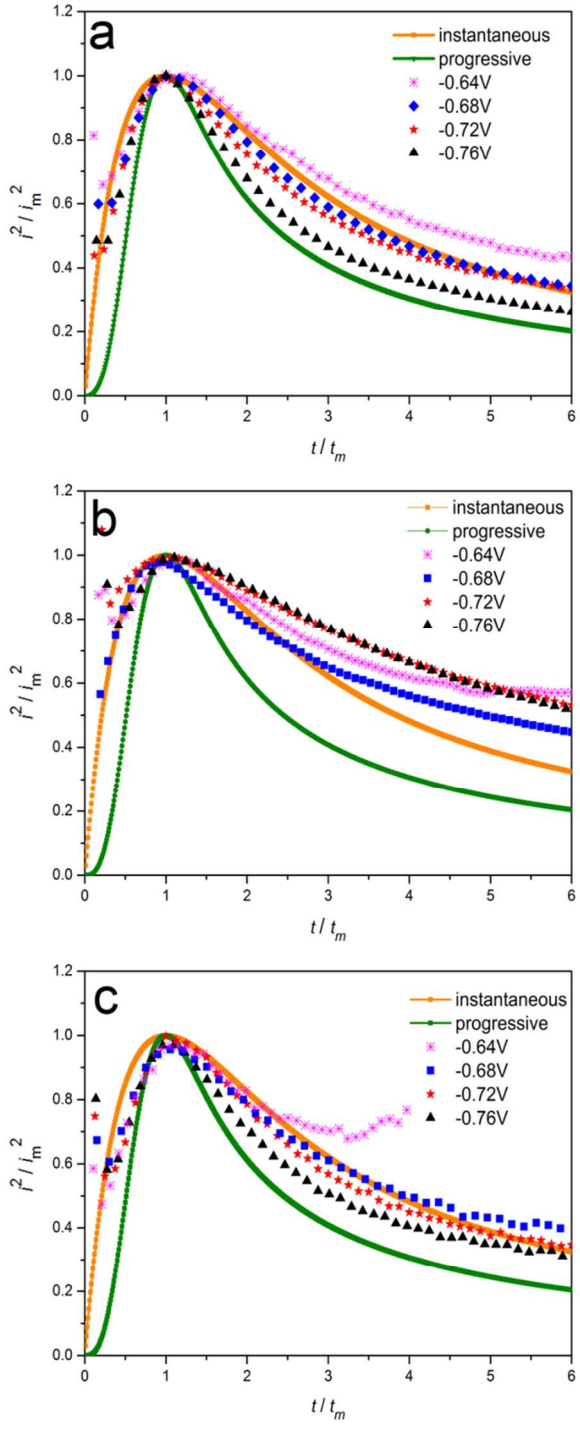

Fig. 4

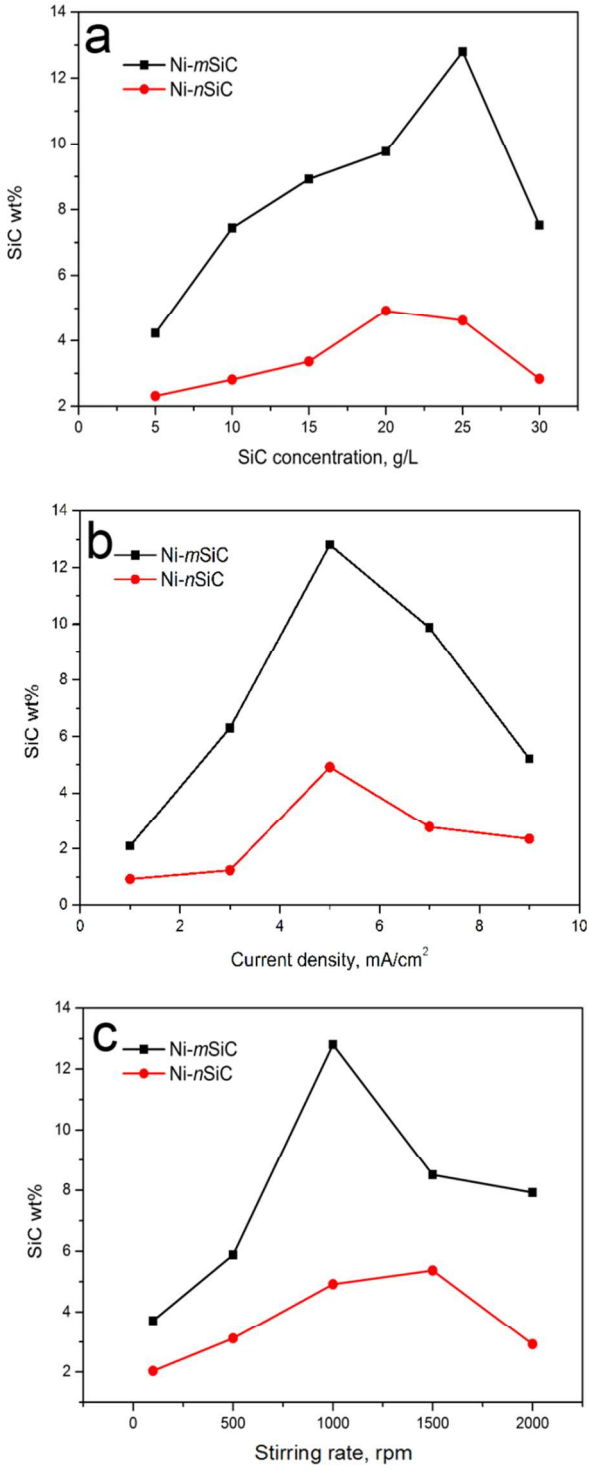

Fig. 5

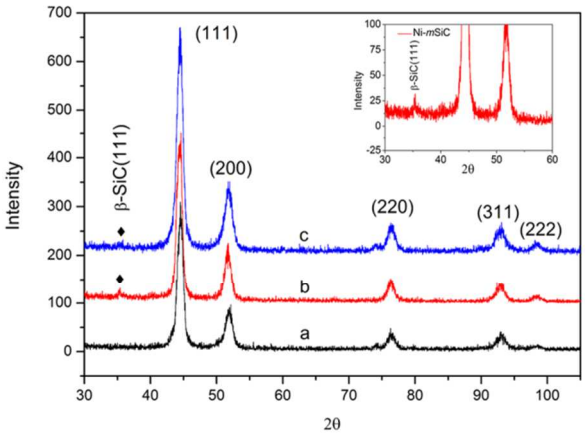

Fig.6

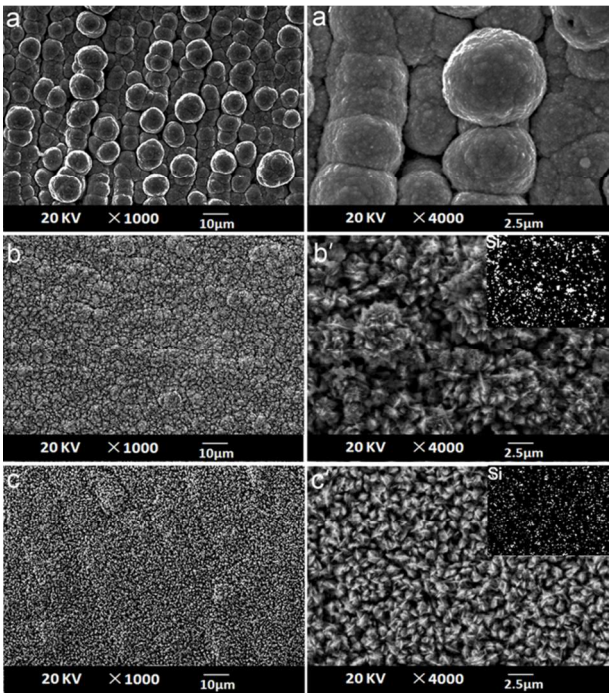

Fig. 7

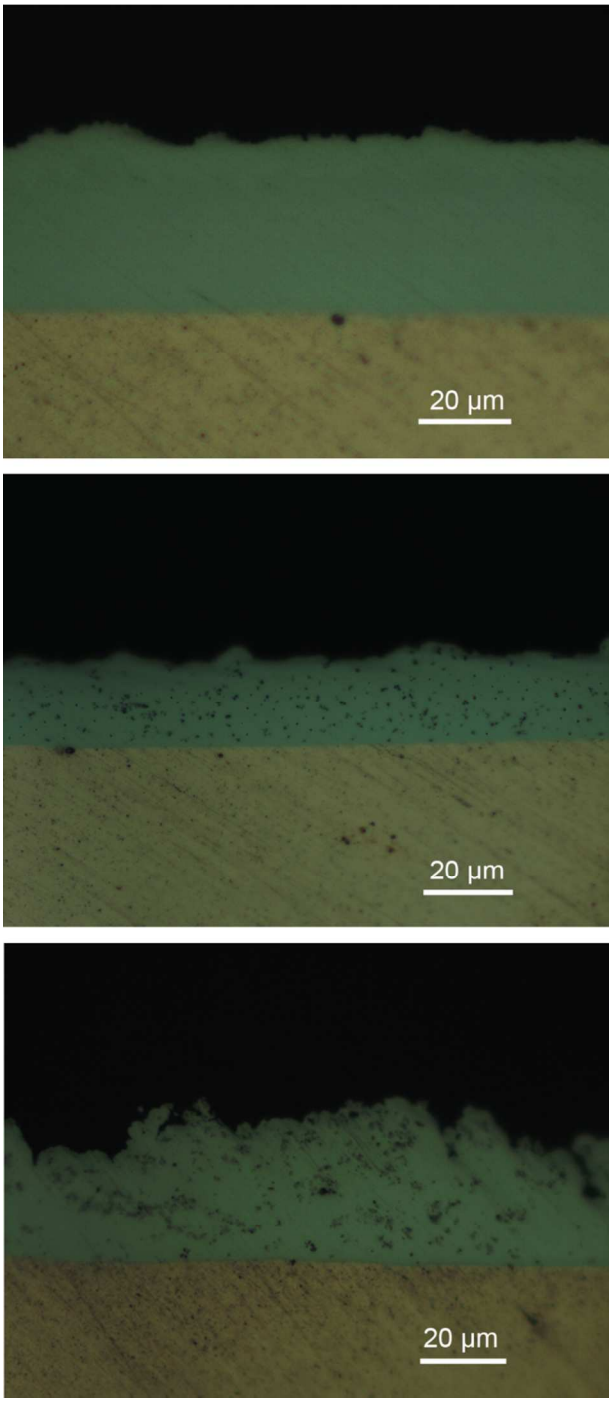

Fig. 8

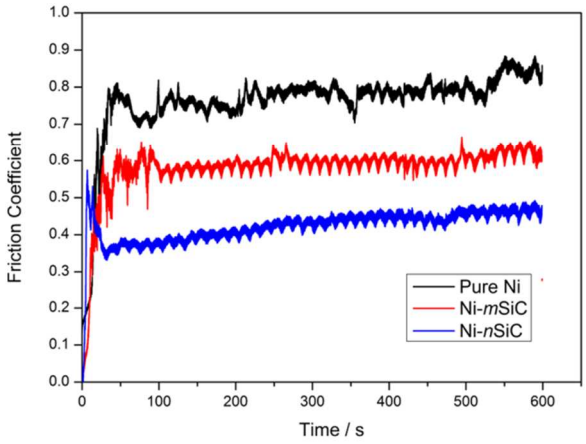

Fig. 9

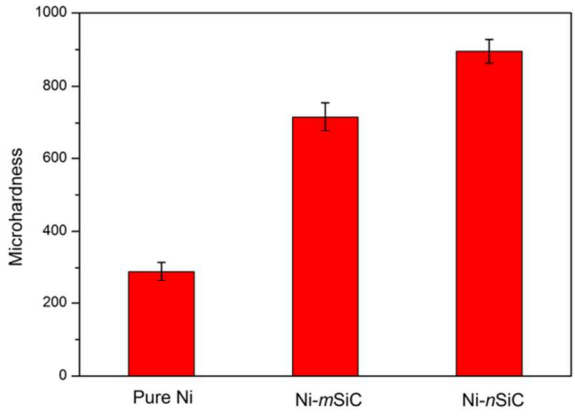

Fig. 10

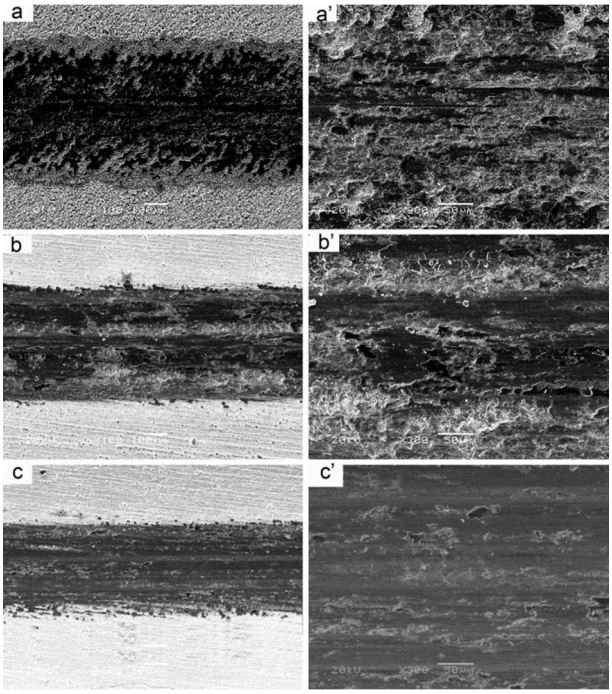

Fig. 11